Phase Transitions

International Edition: DOI: 10.1002/anie.201510024
German Edition: DOI: 10.1002/ange.201510024

Temperature-Induced Irreversible Phase Transition From Perovskite to Diamond But Pressure-Driven Back-Transition in an Ammonium Copper Formate

Ran Shang, Sa Chen, Bing-Wu Wang, Zhe-Ming Wang, and Song Gao**

Abstract: *The compound $[CH_3CH_2NH_3][Cu(HCOO)_3]$ undergoes a phase transition at 357 K, from a perovskite to a diamond structure, by heating. The backward transition can be driven by pressure at room temperature but not cooling under ambient or lower pressure. The rearrangement of one long copper–formate bond, the switch of bridging-chelating mode of the formate, the alternation of N–H···O H-bonds, and the flipping of ethylammonium are involved in the transition. The strong N–H···O H-bonding probably locks the metastable diamond phase. The two phases display magnetic and electric orderings of different characters.*

Apart from their very abundant chemistry,[1] metal–organic frameworks (MOFs) have displayed a rich variety of phase transitions, critical phenomena, and related properties, parallel to conventional materials.[2] The structural, magnetic, electric phase transitions, negative thermal expansion, negative compressibility, amorphization, and framework dynamics, under a change of temperature/pressure, have aroused great interest.[2–8] MOFs thus stand to potentially revolutionize solid-state chemistry and physics.[8a] In this context, ammonium metal formate frameworks (AMFFs) are promising,[9–16] because the combination of ammonium, metal ion, and formate can provide a wide variety of phase transitions via the state alteration of ammonium/formate, and the coupled framework modulation, as well as abundant magnetic, electric, and mechanical properties.[9,10] Several magnetic AMFFs showed coexistence or synergy of magnetic and electric orderings.[11] The $[NH_2NH_3/CH_3NH_3][Mn(HCOO)_3]$ solid solutions display phase transitions modulated by A-site ammonium composition.[12] Negative thermal expansion/negative compressibility have been reported in $[NH_4][M(HCOO)_3]$, $[NH_2NH_3][M(HCOO)_3]$, and $[CH_3NH_3][M(HCOO)_3]$.[11a,d,13] $[tmenH_2][Er(HCOO)_4]_2$ ($tmenH_2^{2+} = [(CH_3)_2NH(CH_2)_2NH(CH_3)_2]^{2+}$) undergoes a pressure ($P$)-induced, reversible phase transformation with the Er–formate bond rearrangement.[14] P-induced phase transitions were evidenced for $[ND_4][Zn(HCOO)_3]$ and $[(CH_2)_3NH_2][Mn(HCOO)_3]$ by spectroscopic studies.[15] Herein, we report a new Cu AMFF,[16] $[CH_3CH_2NH_3][Cu(HCOO)_3]$ (**1**). It undergoes a phase transition at the transition temperature (T_C) of 357 K, from the polar, achiral, low temperature, and high density (LTHD) perovskite to the non-polar, chiral, high-temperature and low-density (HTLD) diamond on heating. Under ambient pressure or lower, the reverse transition could not happen on cooling down to 2 K, but can be induced by compression. The rearrangement of one long copper–formate bond relating to the switch of bridging-chelating modes of the formate, the alternation of N–H···O H-bonds, and the flipping of ethylammonium occur during the transition. The strong N–H···O H-bonds probably lock the metastable HTLD phase below T_C. The two phases show magnetic and electric orderings of different characters in LT region.

The green-blue LTHD crystals of **1** were prepared by a solution method, and the blue HTLD phase was obtained by thermal treatment of LTHD (Experimental Details and Figure S1 in the Supporting Information). In the TGA-DSC runs (Supporting Information, Figure S2), an endothermic peak at 83 °C without weight loss indicated a transition, and the material was thermally stable up to 100 °C. The DSC runs (Figure 1) revealed an irreversible transition under ambient pressure, because LTHD showed an endothermic peak at 357 K in the first heating, but no anomaly in the subsequent cooling-heating cycle, and no anomaly for HTLD. The prominent ΔH and ΔS of 4.9 kJmol^{-1} and 14 Jmol^{-1}K^{-1} indicated a probable first-order transition.[3b,10b,11d] The phase purity was confirmed by powder X-ray diffraction (PXRD; Supporting Information, Figure S3a). The variable-temperature PXRD confirmed the phase transition (Supporting Information, Figure S3b), and the backward transition did not happen down to 2 K under the ambient or lower pressure

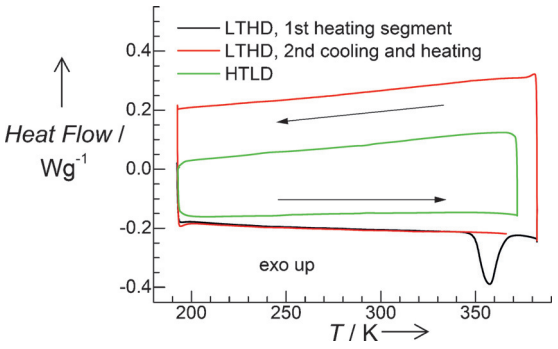

Figure 1. The DSC traces of **1**.

[*] R. Shang, S. Chen, Prof. B.-W. Wang, Prof. Z.-M. Wang, Prof. S. Gao
Beijing National Laboratory for Molecular Sciences, State Key Laboratory of Rare Earth Materials Chemistry and Applications, College of Chemistry and Molecular Engineering, Peking University
Beijing 100871 (China)
E-mail: zmw@pku.edu.cn
gaosong@pku.edu.cn

Supporting information for this article is available on the WWW under http://dx.doi.org/10.1002/anie.201510024.

(Supporting Information, Figure S3c). The HTLD phase was stable at room temperature for long time. However, when the HTLD samples were pressed (0.1 ~ 1.8 GPa), the *P*-driven backward transition to LTHD occurred (Supporting Information, Figure S3 d). Once the pressed sample was heated, it changed to HTLD again. Therefore, the LTHD can transfer to HTLD by heating, while the reverse transition can only be realized by pressing. Compound **1** is a very rare example showing a *T*-induced irreversible transition but *P*-driven backward one, which to the best of our knowledge has never observed before for MOFs.[4,6b]

The single-crystal structures were determined for LTHD (93–340 K) and HTLD (100–360 K; Figure 2; Supporting Information, Figure S4, Tables S1, S2). The LTHD perovskite phase is in the polar, achiral space group $Pna2_1$. It has an anionic copper formate framework of $4^{12}\cdot6^3$ topology, with the

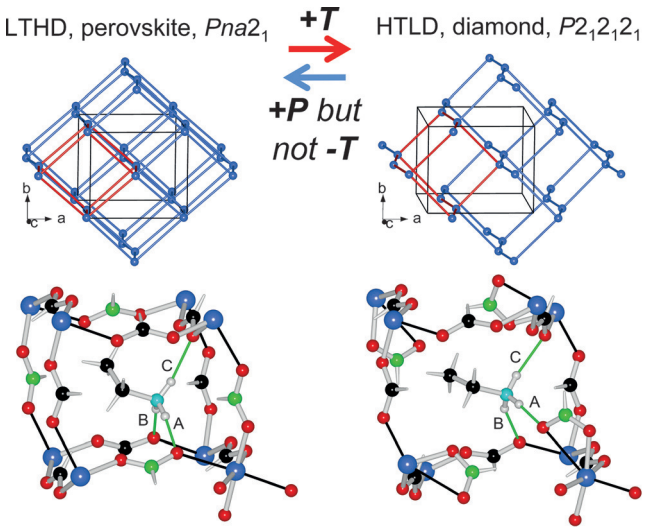

Figure 2. The structures of **1**. Upper: topological views of the frameworks, with cavities highlighted in red. Lower: one ammonium in the framework cavity. The black thin lines are long Cu–O bonds and green lines N–H···O H-bonds labeled A, B, and C. Note the switching of A and C (see text). Cu violet-blue, O red, C green/black for switched/unswitched formate, H white, N cyan, and violet-blue/red sticks for formate bridges in upper views.

$CH_3CH_2NH_3^+$ in the cube-like cavity. The Cu^{2+} ions are connected by *anti-anti* formates. The CuO_6 is a 4 + 2 elongated octahedron, with four short basal Cu–O bonds of 1.960–2.017 Å, and two long apical ones of 2.366 and 2.450 Å at 93 K (the molecular geometries discussed are all at 93 K for LTHD and 100 K for HTLD). The short basal Cu–O bonds form Cu–formate zigzag chains linked by long apical Cu–O bonds,[16] and the chain runs along *c*. In the chain, the neighboring CuO_4 squares are tilted 31°, the Cu···Cu distance is 5.731 Å and the Cu-Cu-Cu angle 167.7°. The inter-chain Cu-OCHO-Cu linkages, in *ab* diagonals, are 6.021 and 6.160 Å. In the cavity, the $CH_3CH_2NH_3^+$ cation lies approximately on the longest body diagonal, and the NH_3^+ end forms three short N–H···O H-bonds to the framework. The cavity volume[17a] of 62 Å^3, matches the vdW size 64 Å^3 of the cation.[17b] From 93 to 340 K the structure showed slight changes in inter-atomic distances, cavity volume and cell dimensions, and slight cell contraction from 320 to 340 K (Supporting Information, Figure S5).

The transition irreversibility upon cooling allowed the HTLD structure determined down to 100 K. The HTLD phase is in the non-polar, chiral space group $P2_12_12_1$. The HTLD cell is 10 % larger than the LTHD one, thus the density 10 % reduced (Supporting Information, Table S1), with *a*-expansion 10 %, *b*-expansion 2 %, but *c*-contraction 2 % (Supporting Information, Figure S5). Therefore, the thermal expansion is significantly anisotropic.[5] The most prominent structure alternation is that the framework changed from LTHD perovskite to HTLD diamond, by a bond rearrangement involving one long apical Cu–O bond. During the transition, this Cu–O bond (Cu–O2 2.366 Å in LTHD) broken, the formate rotated 180°, and the dangling O end retraced to bind to the Cu, forming a longer Cu–O bond (Cu–O1 2.713 Å in HTLD). The bridging formate thus became chelating. Therefore, half number of the edges, in *ab* diagonals, of the LTHD perovskite framework broke, resulting in the HTLD diamond framework of 6^6 topology. The Cu^{2+} is better described as a square pyramid, with four short basal Cu–O bonds of 1.954–2.007 Å (the same basal Cu–O ones in LTHD) and one apical Cu–O bond of 2.262 Å (from the other long apical Cu–O 2.450 Å in LTHD). The copper–formate zigzag chains remain. In the chain the neighboring CuO_4 squares are tilted 44°. The intra-chain Cu···Cu distance is 5.654 Å, and the Cu-Cu-Cu angle 161.4°, both smaller than that in LTHD. The still existing inter-chain Cu-OCHO-Cu edge is 5.843 Å, but 7.247 Å for the broken ones. Such alternations led to the positive thermal expansion along *a* and *b* but negative along *c*, and the copper–formate zigzag chain acts like a spring.[4,5] On the other hand, the observed *P*-driven backward transition implies the positive or normal compressibility along *a* and *b*, but negative along *c*.[5] The HTLD diamondoid cavity combines two LTHD cavities, and the cations of half number have their CH_3 parts flipping to the opposite (Supporting Information, Figure S6). In HTLD the cavity space for one cation is 80 Å^3, 18 Å^3 larger than that in LTHD. On heating the structure remains unchanged, and slight cell contraction occurs from 320 to 360 K. However, the thermal motion of CH_3CH_2 part of the cation enhances more significantly than that in LTHD, given the larger cavity volume in HTLD. The change from bridging to chelating formate has been reported in $[tmenH_2][Er(HCOO)_4]_2$ by pressing,[14] but for **1** this occurs in opposite, chelating to bridging. Significant changes in bond lengths or angles under high pressure were usually observed in MOFs,[2,5,6,8,18] however, *P*-induced bond rearrangement is still scarce.[6b,8b,14]

The changes in N–H···O H-bonds (Figure 2; Supporting Information, Table S2) are interesting, and probably relate to the apparent *T*-irreversibility of the transition. The N–H···O H-bonds labeled A and B in Figure 2 are relevant to the long Cu–O bonds with/without bond rearrangement. They changed from the modest (A)/strong (B) (N···O 2.829/2.778 Å, N–H···O 166.3/172.5°) to the strong (A)/modest (B) (N···O 2.715/2.935 Å, N–H···O 174.1/157.6°) on heating. The former switched from one formate to another, both involved in Cu–O bond rearrangement. The later did not

switch. The third (labeled C) switched between two O atoms of the formate involving short Cu–O bonds. These observations implied that the strong N–H···O H-bonds could prohibit the Cu–O bond rearrangement, thus dynamically locked the metastable HTLD below T_C,[19] resulting in the transition irreversibility down to 2 K under ambient or lower pressure. Since the LTHD phase is denser thus thermodynamically stable[20] below T_C, it is expected that the dynamic locking of the less dense and thermodynamically metastable HTLD could be overcome by pressing,[5] as what has been observed.

The two phases are spin-canted antiferromagnets of different characters (Figure 3a; Supporting Information, Figure S7, Table S3). As both consist of copper–formate chains linked by the secondary Cu–O bonds, the χ vs T data showed broad maxima around 50 K caused by strong intra-chain antiferromagnetic coupling,[16] Below 10 K the traces rose up

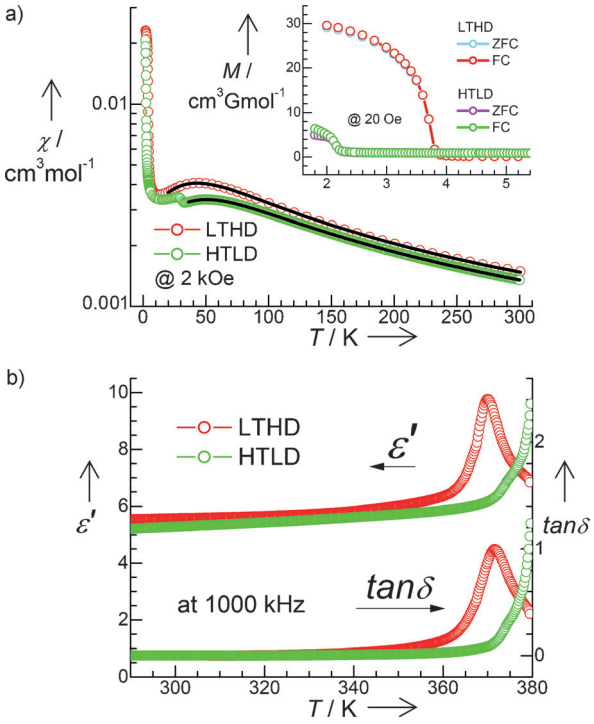

Figure 3. a) Plots of χ vs T under 2 kOe for the two phases. Black lines show the best fittings (see text). Inset: the ZFC/FC plots under 20 Oe. b) $\varepsilon'/\tan\delta$ vs T traces at 1 MHz for the two phases.

quickly. The Curie and Weiss constants are 0.553 cm^3Kmol^{-1}/−71.0 K and 0.498 cm^3Kmol^{-1}/−67.7 K for LTHD and HTLD, respectively (Supporting Information, Figure S7a). The zero-field-cooling and field-cooling (ZFC/FC) runs (Figure 3a, inset), the isothermal magnetizations (Supporting Information, Figure S7b), and the ac susceptibilities (Supporting Information, Figure S7c) confirmed the spin-canted antiferromagnetic orderings. The Néel temperatures (T_N) are 3.7 K (LTHD) and 2.1 K (HTLD). The intra- and inter-chain couplings J and j in cm^{-1}, and g factors, are −46.3(1), −6.2(2) and 2.386(3) for LTHD, and −54.22(4), −4.50(5) and 2.2892-(6) for HTLD, respectively, by simulating the HT susceptibilities with Bonner–Fisher chain model and mean-field correction counting for the inter-chain interaction.[21,22] From LTHD to HTLD, the Cu^{2+} changes from octahedron to square pyramid, its magnetic anisotropy reduces,[23] leading to the smaller g factor, thus smaller susceptibilities and spontaneous magnetizations, and softer magnetism for HTLD. The shorter inter-chain Cu–O bonds result in the larger J, and the reduced inter-chain linkages and the lower density contribute the smaller j, and lower T_N, of HTLD.

The dielectric traces at 1 MHz are shown in Figure 3b. At room temperature the dielectric constant ε' values were 5.5 and 5.2 for LTHD and HTLD, respectively (Supporting Information, Table S3). On heating, the ε' of LTHD increased slowly to 6.4 around 360 K, then quickly rose to a maximum of 9.8 around 370 K, after that it went down. For HTLD, the ε' value increased slowly to 6.2 around 370 K and above 370 K rose more significantly, but above 380 K the response should be effected by the thermal decomposition. The loss $\tan\delta$ at 1 MHz showed the similar behaviors. For lower frequencies (Supporting Information, Figure S8), the dielectric responses display similar features though enhanced. Clearly, the dielectric anomaly for LTHD is due to the phase transition. The LTHD phase is polar and ferroelectric.[11d,e,f] When approaching T_C, the polarization reversal and the domain-wall motion contribute the gradually increased dielectric responses, more significant at lower frequencies.[24] The nucleation of the HTLD phase within the LTHD matrix increases the contribution of domain-wall motion thus further dielectric enhancement. When the phase transition finishes, the dielectric responses drops because the HTLD phase is non-polar or antiferroelectric,[16a] and the local thermal motion of the cations contribute low responses. Both phases showed low and featureless $\varepsilon'/\tan\delta$ on cooling from 300 K (Supporting Information, Figure S9).

In conclusion, the Cu-AMFF **1** undergoes a rare phase transition from a polar, achiral LTHD perovskite to a non-polar, chiral HTLD diamond on heating, but the reverse transition can only be induced by pressure. The transition is accompanied by the rearrangement of one long axial Cu–O bond together with the switch of bridging-chelating modes of the related formate, the changes in N–H···O H-bonds, and the flipping of ammonium. The strong N–H···O H-bonds probably prohibit the Cu–O bond rearrangement, thus dynamically lock the metastable HTLD phase on cooling. Both phases showed coexistence of electric and magnetic orderings in LT region, they thus should be of further interesting for MOF-based multiferroics. This work demonstrates the very wide variety in phase transition and relevant properties of MOFs.

Acknowledgements

This work was supported by the NSFC (Grants 21171010, 91422302, 21290170 and 21290171) and the National Basic Research Program of China (Grant 2013CB933401).

Keywords: ammonium copper formate · magnetism · metal–organic frameworks · perovskite · phase transitions

How to cite: *Angew. Chem. Int. Ed.* **2016**, *55*, 2097 – 2100
Angew. Chem. **2016**, *128*, 2137 – 2140

[1] a) H. Furukawa, U. Müller, O. M. Yaghi, *Angew. Chem. Int. Ed.* **2015**, *54*, 3417 – 3430; *Angew. Chem.* **2015**, *127*, 3480 – 3494; b) H. Deng, C. J. Doonan, H. Furukawa, R. B. Ferreira, J. Towne, C. B. Knobler, B. Wang, O. M. Yaghi, *Science* **2010**, *327*, 846 – 850; c) H.-C. Zhou, J. R. Long, O. M. Yaghi, *Chem. Rev.* **2012**, *112*, 673 – 674; d) J. R. Long, O. M. Yaghi, *Chem. Soc. Rev.* **2009**, *38*, 1213 – 1214; e) S. Hhorike, S. Shimomura, S. Kitagawa, *Nat. Chem.* **2009**, *1*, 695 – 704.

[2] a) I. E. Collings, A. B. Cairns, A. L. Thompson, J. E. Parker, C. C. Tang, M. G. Tucker, J. Catafesta, C. Levelut, J. Haines, V. Dmitriev, P. Pattison, A. L. Goodwin, *J. Am. Chem. Soc.* **2013**, *135*, 7610 – 7620; b) T. D. Bennett, J.-C. Tan, S. A. Moggach, R. Galvelis, C. Mellot-Draznieks, B. A. Reisner, A. Thirumurugan, D. R. Allan, A. K. Cheetham, *Chem. Eur. J.* **2010**, *16*, 10684 – 10690.

[3] a) J. S. Miller, D. Gatteschi, *Chem. Soc. Rev.* **2011**, *40*, 3065 – 3066; b) W. Zhang, R.-G. Xiong, *Chem. Rev.* **2012**, *112*, 1163 – 1195.

[4] a) C. Lind, *Materials* **2012**, *5*, 1125 – 1154; b) A. L. Goodwin, M. Calleja, M. J. Conterio, M. T. Dove, J. S. O. Evans, D. A. Keen, L. Peters, M. G. Tucker, *Science* **2008**, *319*, 794 – 797; c) Y. Wu, A. Kobayashi, G. J. Halder, V. K. Peterson, K. W. Chapman, N. Lock, P. D. Southon, C. J. Kepert, *Angew. Chem. Int. Ed.* **2008**, *47*, 8929 – 8932; *Angew. Chem.* **2008**, *120*, 9061 – 9064.

[5] a) A. B. Cairns, J. Catafesta, C. Levelut, J. Rouquette, A. van der Lee, L. Peters, A. L. Thompson, V. Dmitriev, J. Haines, A. L. Goodwin, *Nat. Mater.* **2013**, *12*, 212 – 216; b) A. B. Cairns, A. Thompson, L. M. G. Tucker, J. Haines, A. L. Goodwin, *J. Am. Chem. Soc.* **2012**, *134*, 4454 – 4456; c) J. M. Ogborn, I. E. Collings, S. A. Moggach, A. L. Thompson, A. L. Goodwin, *Chem. Sci.* **2012**, *3*, 3011 – 3017; d) R. H. Baughman, S. Stafström, C. Cui, S. O. Dantas, *Science* **1998**, *279*, 1522 – 1524.

[6] a) A. B. Cairns, A. L. Goodwin, *Chem. Soc. Rev.* **2013**, *42*, 4881 – 4893; b) F.-X. Coudert, *Chem. Mater.* **2015**, *27*, 1905 – 1916.

[7] T. D. Bennett, A. K. Cheetham, *Acc. Chem. Res.* **2014**, *47*, 1555 – 1562.

[8] a) K. J. Gagnon, C. M. Beavers, A. Clearfield, *J. Am. Chem. Soc.* **2013**, *135*, 1252 – 1255; b) A. U. Ortiz, A. Boutin, K. J. Gagnon, A. Clearfield, F.-X. Coudert, *J. Am. Chem. Soc.* **2014**, *136*, 11540 – 11545.

[9] a) R. Shang, S. Chen, Z. M. Wang, S. Gao in *Metal-Organic Framework Materials* (Eds.: L. R. Macgillivray, C. M. Lukehart), Wiley, Chichester, **2014**; b) Z. M. Wang, K. L. Hu, S. Gao, H. Kobayashi, *Adv. Mater.* **2010**, *22*, 1526 – 1533.

[10] a) L. Cañadillas-Delgado, O. Fabelo, J. A. Rodríguez-Velamazán, M. Lemée-Cailleau, S. A. Mason, E. Pardo, F. Lloret, J. Zhao, X. Bu, V. Simonet, C. V. Colin, J. Rodríguez-Carvajal, *J. Am. Chem. Soc.* **2012**, *134*, 19772 – 19781; b) R. Shang, Z. M. Wang, S. Gao, *Angew. Chem. Int. Ed.* **2015**, *54*, 2534 – 2537; *Angew. Chem.* **2015**, *127*, 2564 – 2567; c) R. Shang, G. C. Xu, Z. M. Wang, S. Gao, *Chem. Eur. J.* **2014**, *20*, 1146 – 1158; d) R. Shang, S. Chen, K. L. Hu, Z. C. Jiang, B. W. Wang, M. Kurmoo, Z. M. Wang, S. Gao, *APL Mater.* **2014**, *2*, 124104.

[11] a) G.-C. Xu, W. Zhang, X.-M. Ma, Y.-H. Chen, L. Zhang, H.-L. Cai, Z.-M. Wang, R.-G. Xiong, S. Gao, *J. Am. Chem. Soc.* **2011**, *133*, 14948 – 14951; b) D.-W. Fu, W. Zhang, H.-L. Cai, Y. Zhang, J.-Z. Ge, R.-G. Xiong, S. D. Huang, T. Nakamura, *Angew. Chem. Int. Ed.* **2011**, *50*, 11947 – 11951; *Angew. Chem.* **2011**, *123*, 12153 – 12157; c) P. Jain, V. Ramachandran, R. J. Clark, H. D. Zhou, B. H. Toby, N. S. Dalal, H. W. Kroto, A. K. Cheetham, *J. Am. Chem. Soc.* **2009**, *131*, 13625 – 13627; d) S. Chen, R. Shang, K. L. Hu, Z. M. Wang, S. Gao, *Inorg. Chem. Front.* **2014**, *1*, 83 – 98; e) D. Di Sante, A. Stroppa, P. Jain, S. Picozzi, *J. Am. Chem. Soc.* **2013**, *135*, 18126 – 18130; f) A. Stroppa, P. Jain, P. Barone, M. Marsman, J. M. Perez-Mato, A. K. Cheetham, H. W. Kroto, S. Picozzi, *Angew. Chem. Int. Ed.* **2011**, *50*, 5847 – 5850; *Angew. Chem.* **2011**, *123*, 5969 – 5972.

[12] S. Chen, R. Shang, B. W. Wang, Z. M. Wang, S. Gao, *Angew. Chem. Int. Ed.* **2015**, *54*, 11093 – 11096; *Angew. Chem.* **2015**, *127*, 11245 – 11248.

[13] a) W. Li, M. R. Probert, M. Kosa, T. D. Bennett, A. Thirumurugan, R. P. Burwood, M. Parinello, J. A. K. Howard, A. K. Cheetham, *J. Am. Chem. Soc.* **2012**, *134*, 11940 – 11943; b) Z. M. Wang, B. Zhang, T. Otsuka, K. Inoue, H. Kobayashi, M. Kurmoo, *Dalton Trans.* **2004**, 2209 – 2216.

[14] E. C. Spencer, M. S. R. N. Kiran, W. Li, U. Ramamurty, N. L. Ross, A. K. Cheetham, *Angew. Chem. Int. Ed.* **2014**, *53*, 5583 – 5586; *Angew. Chem.* **2014**, *126*, 5689 – 5692.

[15] a) M. Mączka, P. Kadłubański, P. T. C. Freire, B. Macalik, W. Paraguassu, K. Hermanowicz, J. Hanuza, *Inorg. Chem.* **2014**, *53*, 9615 – 9624; b) M. Mączka, T. A. da Silva, W. Paraguassu, M. Ptak, K. Hermanowicz, *Inorg. Chem.* **2014**, *53*, 12650 – 12657.

[16] a) R. Shang, S. Chen, Z. M. Wang, S. Gao, *Chem. Eur. J.* **2014**, *20*, 15872 – 15883; b) Z. Wang, P. Jain, K.-Y. Choi, J. van Tol, A. K. Cheetham, H. W. Kroto, H.-J. Koo, H. Zhou, J. Hwang, E. S. Choi, M.-H. Whangbo, N. S. Dalal, *Phys. Rev. B* **2013**, *87*, 224406; c) M.-Y. Li, M. Kurmoo, Z. M. Wang, S. Gao, *Chem. Asian J.* **2011**, *6*, 3084 – 3096; d) K.-L. Hu, M. Kurmoo, Z.-M. Wang, S. Gao, *Chem. Eur. J.* **2009**, *15*, 12050 – 12064.

[17] a) A. L. Spek, PLATON, *A Multipurpose Crystallographic Tool*, Utrecht University, Utrecht, The Netherland, **2001**; b) PCMODEL Version 9.1, see http://www.serenasoft.com.

[18] a) J. A. Gould, M. J. Rosseinsky, S. A. Moggach, *Dalton Trans.* **2012**, *41*, 5464 – 5467; b) P. Parois, S. A. Moggach, A. R. Lennie, J. E. Warren, E. K. Brechin, M. Murrie, S. Parsons, *Dalton Trans.* **2010**, *39*, 7004 – 7011.

[19] E. Boldyreva, *Cryst. Growth Des.* **2007**, *7*, 1662 – 1668.

[20] J. Bernstein, *Polymorphism in Molecular Crystals*, Oxford University Press, Oxford, **2002**, pp. 40 – 41.

[21] a) W. E. Estes, D. P. Gavel, W. E. Hatfield, D. Hodgson, *Inorg. Chem.* **1978**, *17*, 1415 – 1421; b) O. Kahn, *Molecular Magnetism*, Wiley-VCH, New York, **1993**, p. 252.

[22] R. L. Carlin, *Magnetochemistry*, Springer, Heidelberg, **1986**, p. 133.

[23] A. T. Casey, S. Mitra in *Theory and Application of Molecular Paramagnetism* (Eds.: L. N. Mulay, E. A. Boudreaux), Wiley, New York, **1976**, pp. 234 – 243.

[24] M. E. Lines, A. M. Glass, *Principles and Applications of Ferroelectrics and Related Materials*, Clarendon, Oxford, **1977**.

Received: October 27, 2015
Published online: December 28, 2015

